Key Engineering Materials
ISSN: 1662-9795, Vol. 1047, pp 223-230

Submitted: 2026-01-19
Revised: 2026-02-18
Accepted: 2026-02-25
Online: 2026-04-13

Feasibility of Direct 3D Printing Foam Polylactic Acid with MEX

Batagiannis Athanasios[1,a], Panagiotis Karmiris-Obratański[2,b], Ioannis T. Christodoulou[1,c], Emmanouil L. Papazoglou[1,d], Angelos P. Markopoulos[1,e*]

[1]School of Mechanical Engineering - Laboratory of Manufacturing Technology, National Technical University of Athens, Athens, Greece

[2]Advanced Manufacturing Laboratory, Department of Manufacturing Systems, Faculty of Mechanical Engineering and Robotics, AGH University of Krakow, Krakow, Poland

[a]batagiannis.a@gmail.com, [b]karmiris@agh.edu.pl, [c]ichristodoulou@mail.ntua.gr, [d]mlpapazoglou@gmail.com, [e*]amark@mail.ntua.gr

Keywords: material extrusion (MEX), PLA – foam PLA, different temperatures – flow rates, tensile properties.

Abstract. Additive manufacturing of polymeric foams via Material Extrusion (MEX) is an attractive route to lightweight components with tunable mechanical response. However, reproducible performance remains challenging because foam expansion, cell stabilization, and inter-layer bonding are strongly governed by the thermal–processing window. This study evaluates the feasibility of directly printing a commercial PLA foaming filament and quantifies the influence of nozzle temperature (and the associated flow-rate adjustment) on density and tensile behavior. ISO 527-2 tensile specimens were printed under three printing-condition combinations, a nominal PLA setting (190°C, 100% flow) and two foaming-window settings (250°C, 55% flow and 270°C, 50% flow). Tensile tests were conducted, and the tensile properties were assessed via Young's Modulus, Yield and Ultimate properties (stress/strain), and elastic and total absorbed energy up to fracture. In addition to absolute values, all relevant metrics were normalized by relative density to enable robust comparisons across foaming levels. Finally, the DIC maps at the Yield and Fracture point were used to support the derived results and conclusions.

Introduction

Additive manufacturing (AM) of polymeric foams is attracting increasing interest due to its ability to merge layer-wise fabrication with cellular material architectures [1,2]. This integration gives the ability to develop lightweight components with tunable mechanical performance [3]. AM allows precise control over part morphology and internal porosity, which is difficult to achieve using conventional foam manufacturing routes due to its geometric freedom [4].

Among the available AM techniques, material extrusion (MEX)—widely known as fused filament fabrication (FFF)—is one of the most established and commercially prevalent technologies [5]. In MEX, three-dimensional components are fabricated directly from computer-aided design (CAD) data through the sequential deposition of molten thermoplastic material. Compared with traditional manufacturing techniques, MEX offers superior design flexibility, cost-effective fabrication of complex geometries, rapid production cycles, and straightforward customization using relatively low-cost materials and equipment [6].

Despite its technological maturity, the application of MEX to polymeric foams remains comparatively underexplored, particularly with regard to the controlled generation of cellular structures during the printing process [7]. The introduction of foaming agents and mechanisms within the extrusion stage enables the fabrication of lightweight components with reduced material consumption and enhanced functional performance [8]. However, the resulting foam morphology and mechanical behavior are strongly influenced by the type and size of the foaming agent, as well as the printing parameters and thermal history, which govern gas expansion, cell stabilization, and interlayer adhesion [9]. Damanpack, Sousa and Bodaghi [10] investigated the influence of printing temperature and flow rate

on the tensile mechanical properties and porosity of the printed samples. The authors developed an analytical model that can correlate the mechanical properties with the porosity of PLA foams. In the study by Abu Hassan et al. [11] investigated the influence of the foaming agent and the printing temperature on the properties of PLA/kenaf composites. The findings show that lower extrusion temperatures promote finer and more uniform cell structures, although this was accompanied by a reduction in mechanical properties.

Based on the abovementioned, a systematic investigation of the relationship between processing conditions and foam characteristics is essential to ensure reproducibility and performance consistency in additively manufactured polymeric foams, given that even small variations in printing temperature can lead to measurable changes in material properties. The present study examines the influence of nozzle temperature on the resulting density and tensile performance of a PLA foaming filament. Three printing temperatures were selected: one close to the nominal processing temperature of conventional PLA and two within the material's foaming window, in conjunction with appropriate adjustments of the flow rate. The tensile response was characterized in terms of Young's Modulus (YM), Yield Stress (YS) and the corresponding Yield Strain (YStr), Ultimate Tensile Strength (UTS) and the corresponding Ultimate Tensile Strain (UTStr), as well as the Total absorbed Energy up to fracture (TE) and the Elastic Energy (EE). In addition to the absolute values, density-normalized properties were calculated using the relative density, enabling more robust comparisons across foaming conditions. Finally strain data obtained via digital image correlation (DIC) were also used to support the assessment of the material's tensile behavior.

Materials and Methods

The specimen geometry followed BS EN ISO 527-2:2012 and the parts were fabricated via material extrusion (MEX) on a Flashforge Creator 3 using 1.75 mm PLA foaming filament. The "Standard" slicing profile was employed with a 0.8 mm nozzle. Specifically, a fixed layer-height strategy was adopted with a nominal layer height of 0.30 mm and an increased first-layer height of 0.40 mm. The perimeter configuration employed three shells (nominal shell thickness ≈2.40 mm) with 10% perimeter overlap, and seam placement was controlled via start-point selection ("closest to specific location"). Full-density infill (100%) was used with a line pattern (start angle 45°, cross angle 90°), combined with 4 top solid layers and 3 bottom solid layers and a 15% infill–perimeter overlap, whilst the infill combining option was disabled (maximum solid and sparse combine = 1). The base print speed was 60 mm/s with a travel speed of 100 mm/s, a minimum speed of 20 mm/s, and the first layer printing speed was limited to 40 mm/s. Finally, the exterior wall speed was capped at 40 mm/s and interior wall maximum speeds were set to 60 mm/s. Keeping in mind that the aim of the present work is to investigate the effect of printing temperature on the tensile properties of 3D-printed PLA foaming material, three nozzle temperature – flow rate combinations were examined. The tested conditions spanned from the typical PLA processing window (190°C at 100% flow rate) up to a high-temperature, reduced-flow regime (250°C at 55% flow rate and 270°C at 50%).

The tensile properties were quantified in terms of YM, YS and the corresponding YStr, UTS and the corresponding UTStr, as well as the TE up to fracture and the EE. Since specimens produced at elevated nozzle temperatures exhibit significant foaming, and thus reduced density, direct comparison of the as-measured tensile properties based solely on absolute values is not meaningful. Therefore, in addition to reporting the absolute properties, all values (YM, YS, UTS, EE and TE) were normalized with respect to the relative density of the specimens for each printing condition. The relative density was defined as the ratio of the specimen nominal density to the nominal density of solid PLA (1.24 g/cm^3 [12]). The specimen nominal density was calculated by dividing the experimentally measured mass by the CAD-based specimen volume (8.55 cm^3). Any deviations between the manufactured specimen dimensions and the CAD geometry were considered minor and are not expected to materially affect the results or the conclusions drawn.

Finally, all tensile tests were performed using a Shimadzu universal testing machine equipped with a 20 kN load cell and an optical extensiometer for precise strain acquisition, utilizing a 16 MP CCD camera operating at 5 fps. The tensile loading rate was set to 2 mm/min. Additionally, Digital Image

Correlation (DIC) software (xsight) was employed to obtain full-field strain maps and to validate the strain measurements acquired by the optical extensiometer, enabling a detailed analysis of strain localization and deformation evolution during loading. For this purpose, each specimen was prepared by applying a uniform white matte primer coating (plastic skin), followed by the deposition of a random black speckle pattern on the gauge section to ensure adequate image contrast and reliable DIC correlation throughout the test.

Results and Discussion

Table 1 summarizes the measured tensile metrics and the corresponding relative-density-normalized values for all printing conditions.

Table 1. Tensile properties and the respective reduced to relative density values.

	Rel. Density	YM (MPa)	YS (MPa)	TYStr	UTS (MPa)	UTStr	EE (MJ/m³)	PE (MJ/m³)	TE (MJ/m³)
T190	80%	543	16.11	2.23%	16.876	2.85%	0.22	1.77	2.00
T250	40%	173	5.45	1.61%	5.951	2.33%	0.06	1.85	1.92
T270	41%	213	4.95	2.31%	5.426	24.90%	0.06	1.23	1.29
		Reduced to relative density tensile properties							
T190	80%	677	20.09	2.23%	21.05	2.85%	0.28	2.21	2.49
T250	40%	431	13.54	1.61%	14.79	2.33%	0.16	4.61	4.77
T270	41%	524	12.17	2.31%	13.35	24.90%	0.16	3.02	3.18

In Fig. 1 the dominant role of foaming-induced density reduction on stiffness is presented, while also indicating an additional temperature-dependent microstructural effect beyond density alone. The relative density decreases markedly from ~0.80 at T190 to ~0.40–0.41 at T250 – T270, consistent with strong in situ cell nucleation and expansion at elevated nozzle temperatures and reduced flow rate. This density drop is reflected in the absolute Young's modulus, which falls from 543 MPa (T190) to 173 MPa (T250) and 213 MPa (T270). However, after normalization by relative density, the reduced YM remains lower for the foamed conditions (677 MPa at T190 versus 431 and 524 MPa at T250 and T270 respectively), implying that the stiffness loss cannot be attributed solely to reduced solid fraction. This behavior may be explained by three main reasons. The transition from a predominantly solid "skin–core" structure at T190 to a more compliant cellular core at higher temperatures, the increased inter-layer compliance due to gas expansion during deposition and reduced effective interlayer adhesion area, and possible changes in crystallinity/thermal history that alter the intrinsic stiffness of the polymer matrix. Notably, T250 and T270 exhibit nearly identical relative density but different modulus values, suggesting that the foam morphology (cell size distribution, cell-wall thickness, and degree of coalescence) along with the interlayer bonding quality vary with nozzle temperature even at similar bulk density, thereby modulating stiffness.

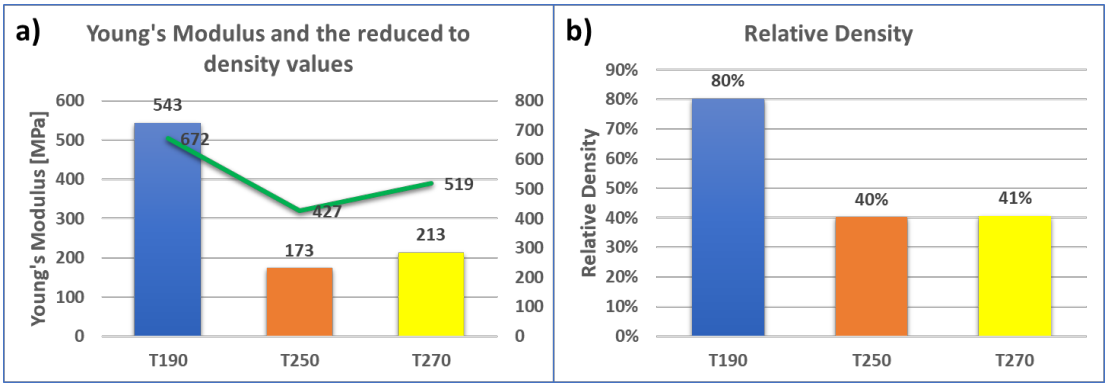

Fig. 1. a) Young's Modulus (bar charts), reduced Young's Modulus (line) and b) Relative density for the different printing temperatures.

Based on the data presented in Fig. 2, yielding is highly sensitive to both density reduction and the thermo-foaming regime, since strength is degrading more than can be explained by density alone. The YS decreases from 16.11 MPa (T190) to 5.45 MPa (T250) and 4.95 MPa (T270), consistent with reduced load-bearing cross-section and stress concentrations introduced by pores. Density normalization partially collapses this trend but does not eliminate it since the reduced YS drops from 20.09 MPa (T190) to 13.54 MPa (T250) and 12.17 MPa (T270), indicating that the effective yield mechanism is additionally governed by microstructural integrity like the cell-wall continuity, the interlayer bonding quality and the void morphology.

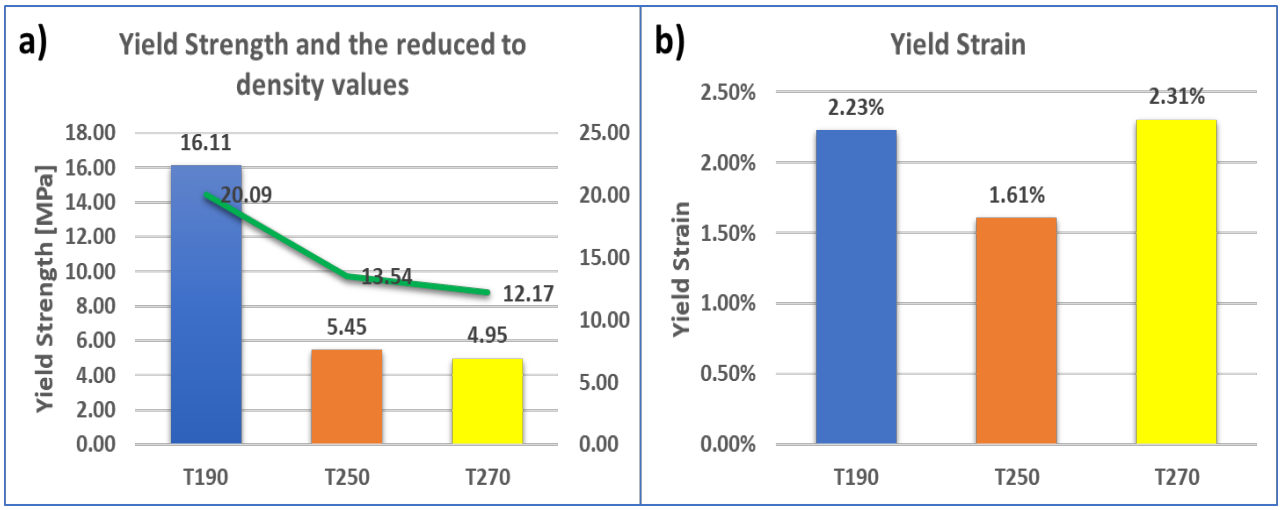

Fig. 2. a) Yield Strength (bar charts), reduced Yield Strength (line) and b) Yields Strain for the different printing temperatures.

The YStr behavior is also interesting since T250 exhibits the lowest YStr (1.61%), implying earlier onset of irreversible deformation, possibly due to weaker bonding and more heterogeneous porosity, whereas T270 shows a higher YStr (2.31%), suggesting a shift toward more stable pre-yield deformation and delayed yielding due to improved chain mobility and interdiffusion at the highest nozzle temperature partially counteracting the foaming-induced heterogeneity. Overall, the combined trends support the interpretation that higher-temperature printing generates a more compliant, porosity-dominated structure with reduced yield capacity, while the yield strain reflects the balance between foam morphology and thermal crystallinity effects that promote a more uniform deformation. In Fig. 3, a significant reduction in tensile strength with foaming is presented, accompanied by a substantial change in post-yield deformation capacity, especially at the highest nozzle temperature. The UTS drops from 16.876 MPa (T190) to 5.951 MPa (T250) and 5.426 MPa (T270), consistent with the lower effective load-bearing area and premature damage initiation at pores and inter-road defects. Normalization by relative density again reduces, but does not remove, the differences (21.05 MPa at T190 versus 14.79 MPa at T250 and 13.35 MPa at T270), reinforcing that the strength reduction is not purely a density effect and likely reflects reduced interlayer bonding efficiency, larger and less uniform cells, and earlier microcrack nucleation at cell-wall junctions. In contrast, the ultimate strain shows a qualitatively different response. More specifically, while T190 and T250 exhibit low UTStr (~2–3%), T270 shows a notably high UTStr (24.90%), suggesting a transition from relatively brittle and limited-strain failure to a highly ductile, stable deformation regime. Mechanistically, this response can arise from a more extensible foam network in which deformation proceeds through progressive cell-wall stretching and reorientation. In this regime, the UTS shifts away from the initial elastic region and occurs at higher strains, closer to the final fracture strain, indicating that the material exhibits limited strain hardening up to fracture.

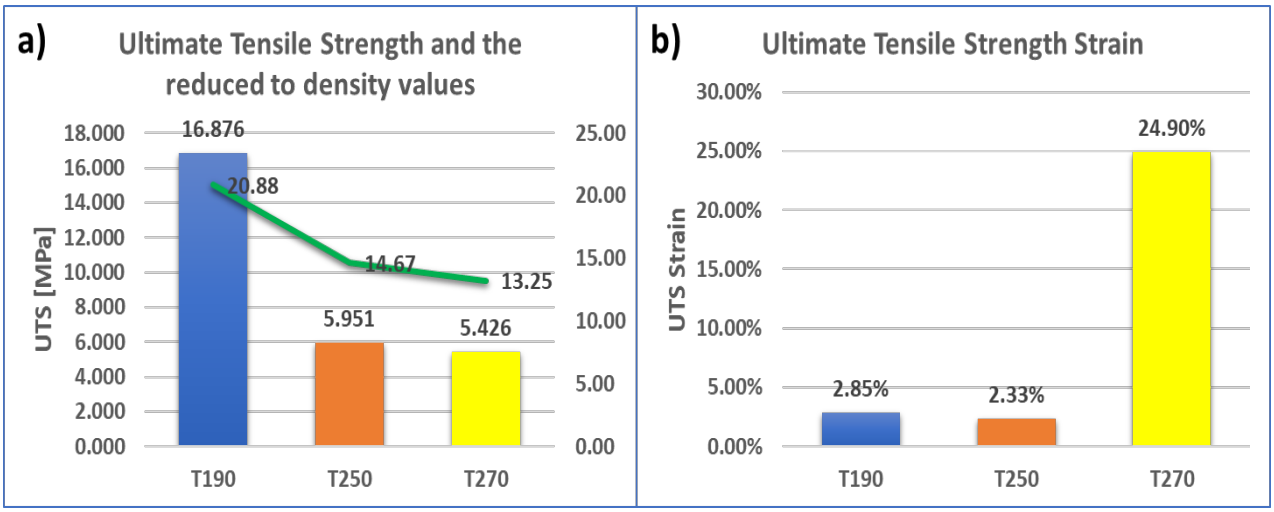

Fig. 3. a) UTS (bar charts), reduced UTS (line) and b) UTStr for the different printing temperatures.

Finally, Fig. 4 consolidates the mechanical implications of foaming by separating stiffness-dominated energy storage from the overall energy absorption capacity up to fracture, and it reveals that density normalization can invert the interpretation of "performance". The EE is highest for the dense material (0.22 MJ/m³ at T190) and drops to 0.06 MJ/m³ for both foamed conditions, which is expected because EE scales strongly with YM and YS / YStr, which have both been reduced by porosity. The absolute TE remains comparable between T190 (2.00 MJ/m³) and T250 (1.92 MJ/m³) but decreases at T270 (1.29 MJ/m³), indicating that excessive foaming and/or microstructural degradation at the highest temperature reduces the material's ability to sustain load over large deformations before fracture. However, once normalized by relative density, TE increases substantially for the foamed conditions (2.49 MJ/m³ at T190 versus 4.77 MJ/m³ at T250 and 3.18 MJ/m³ at T270), implying that, per unit solid material, the foamed architectures can dissipate more energy, a conclusion consistent with progressive damage mechanisms that are efficient energy sinks in cellular polymers. The fact that T250 provides the highest density-normalized TE suggests it offers the most favorable compromise between creating a cellular structure (enhancing energy dissipation per unit mass) and preserving sufficient integrity to avoid premature catastrophic failure, whereas T270, limits absolute and normalized energy absorption despite increased ductility indicators.

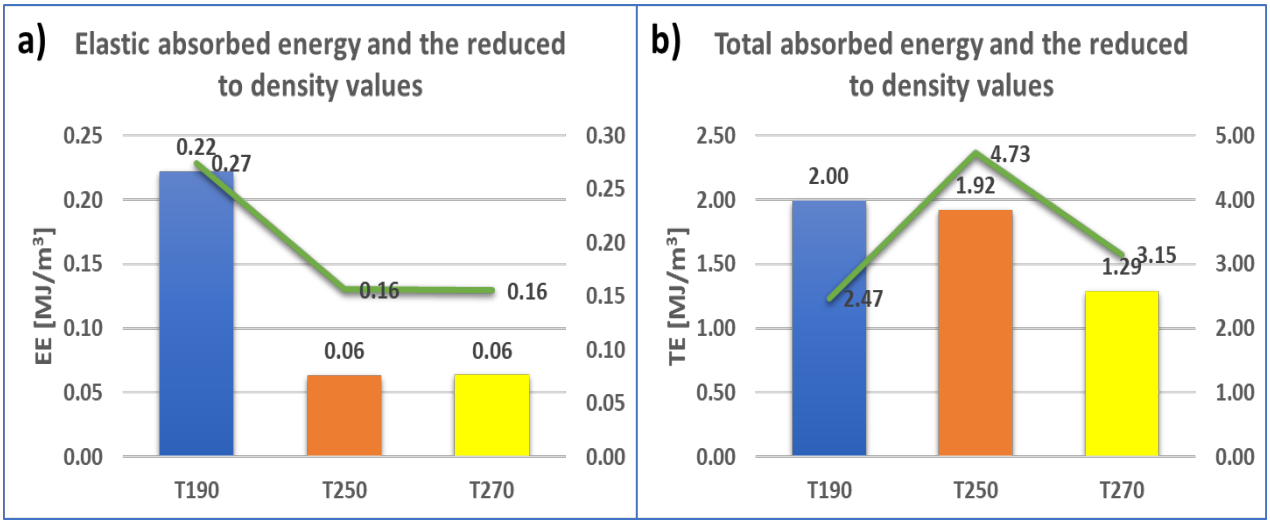

Fig. 4. a) Elastic absorbed energy (bar charts), reduced Elastic absorbed energy (line) and b) Total absorbed energy (bar charts), reduced Total absorbed energy (line) for the different printing temperatures.

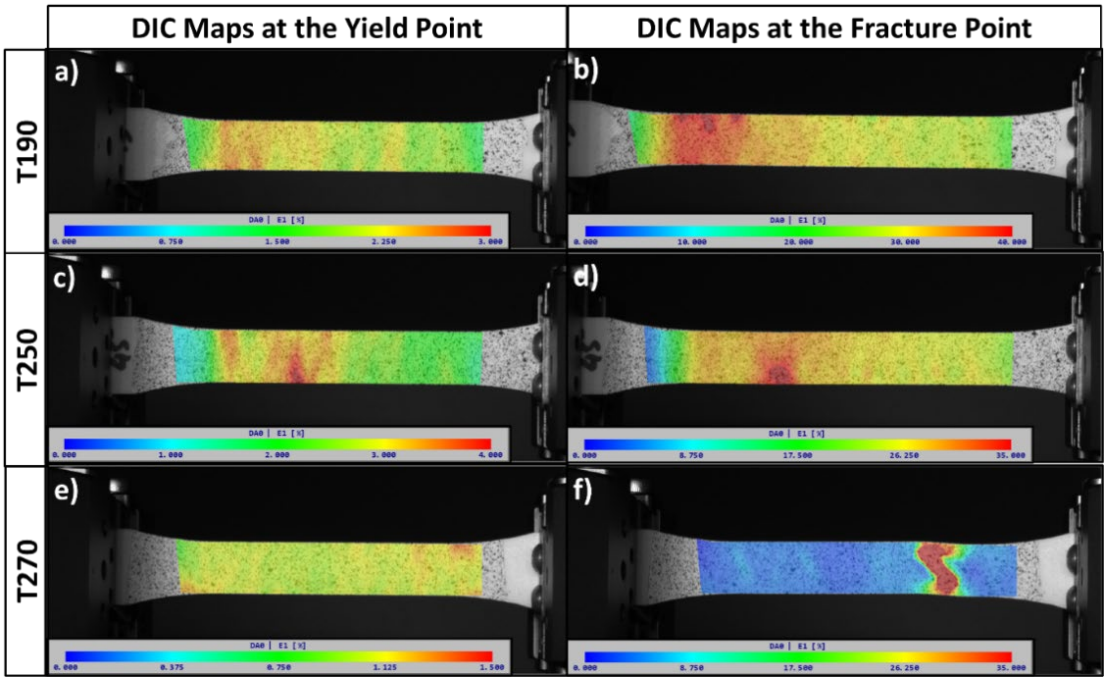

Fig. 5. DIC maps for the different printing temperatures at the (a), (c) and (e) Yield Point and (b), (d) and (f) at the fracture point.

The DIC maps of axial strain e_1 in Fig. 5 provide direct evidence that the deformation mode transitions from largely uniform straining at the nominal PLA temperature (T190) to increasingly heterogeneous and localized deformation as the printing temperature enters the foaming window. At the Yield Point, the low-temperature condition of T190 exhibits a comparatively homogeneous strain field across the gauge section, which is consistent with stable load transfer and limited early strain localization. In contrast, the foamed conditions (T250 and T270) show clear strain gradients and banding and local "hot spots," indicating that yielding initiates preferentially in regions of locally reduced stiffness and strength (e.g., pore-rich zones, thinner cell walls, and weaker inter-layer adhesion). At the fracture point, the high-temperature foamed specimens (T250 and T270) develop substantially larger strains prior to rupture, with a broad region of elevated strain followed by the emergence of a dominant necking failure band, behavior that is consistent with progressive cell-wall stretching, bending, and reorientation and with gradual damage accumulation rather than abrupt catastrophic cracking. Conversely, the low temperature specimen (T190) fractures shortly after yielding, a result in agreement with the small yield-to-fracture strain gap reported in Table 1, whilst the final map is dominated by a narrow high-strain zone at the crack path. This pattern is typical of rapid localization and limited plastic redistribution, while the very high strain values at the immediate fracture line should be interpreted cautiously as they may be amplified by DIC decorrelation during crack initiation and opening.

To close the Results and Discussion section, it is worth noting a few limitations and directions for future work. First, the foaming response was evaluated mainly through bulk density and mechanical/DIC data, without direct microstructural quantification. Measurements of cell-size distribution, porosity fraction, cell-wall thickness, and possible skin–core gradients would strengthen the process–morphology correlation. Second, inter-layer bonding was assessed indirectly, while fracture-surface analysis and interfacial characterization could clarify bonding mechanisms in directly printed MEX foams. Finally, only three nozzle-temperature conditions (with corresponding flow-rate adjustments) and a single material were examined, so the findings should be interpreted within this parameter window and may not directly generalize to other systems. Future work should therefore combine systematic process mapping with quantitative morphology and bonding assessment to further reinforce the process–structure–property link.

Conclusion

In the current study, the effect of nozzle temperature, together with the corresponding flow-rate adjustment, on the foaming intensity and tensile response of material-extruded PLA foaming filament was investigated. ISO 527-2 tensile specimens were printed at one nominal PLA condition and two conditions within the foaming window. The tensile behavior was quantified via YM, YS, YStr, UTS, UTStr, EE and TE, supported by full-field DIC strain mapping. To enable meaningful comparisons across markedly different foam contents, the measured properties were additionally normalized by the relative density derived from specimen mass and CAD volume. Overall, nozzle temperature was shown to be an effective process lever to tune density and mechanical performance, while the results also demonstrate that small thermal shifts within the foaming window can lead to substantial changes in deformation mode and failure characteristics. More specifically, the main conclusions were:

- Increasing nozzle temperature from the nominal PLA setting into the foaming window produced a pronounced reduction in relative density, confirming strong process sensitivity of cellular expansion. This density shift is the primary driver for the reduction of stiffness and strength in absolute terms.
- Density normalization reduced, but did not eliminate, differences in YM and strength between the processing conditions. This indicates that foam morphology and inter-layer bonding quality influence the effective load-bearing efficiency in addition to bulk solid fraction.
- The highest-temperature condition (T270) promoted substantially larger tensile strains prior to fracture, consistent with a more extensible cellular network and progressive cell-wall deformation. DIC maps corroborated this by showing a transition from comparatively uniform straining at nominal temperature to stronger strain localization and band formation in the foamed conditions.
- In absolute terms, EE decreased strongly with foaming due to the reduction in stiffness, while TE depended on the balance between ductility and premature damage. When normalized by relative density, the foamed conditions exhibited improved energy absorption per unit solid material, highlighting the potential of controlled foaming for lightweight, energy-dissipative applications.

References

[1] K. Monkova, P.P. Monka, D. Godec, M. Torokova, Research into the Influence of Volume Fraction on the Bending Properties of Selected Thermoplastic Cellular Structures from a Mechanical and Energy Absorption Perspective, Polymers 17 (2025) 2795. https://doi.org/10.3390/polym17202795.

[2] T. Standau, C. Zhao, S. Murillo Castellón, C. Bonten, V. Altstädt, Chemical Modification and Foam Processing of Polylactide (PLA), Polymers 11 (2019) 306. https://doi.org/10.3390/polym11020306.

[3] K. Kalia, B. Francoeur, A. Amirkhizi, A. Ameli, In situ foam 3D printing of microcellular structures using material extrusion additive manufacturing, ACS Appl. Mater. Interfaces 14 (2022) 22454–22465. https://doi.org/10.1021/acsami.2c03014.

[4] W. Gao, Y. Zhang, D. Ramanujan, K. Ramani, Y. Chen, C.B. Williams, et al., The status, challenges, and future of additive manufacturing in engineering, Comput.-Aided Des. 69 (2015) 65–89. https://doi.org/10.1016/j.cad.2015.04.001.

[5] K. Monkova, P.P. Monka, J. Burgerova, G. Szabo, Investigating the Flexural Properties of 3D-Printed Nylon CF12 with Respect to the Correlation Between Loading and Layering Directions, Polymers 17 (2025) 788. https://doi.org/10.3390/polym17060788.

[6] K. Rydzoń, Mechanical properties of body centered cubic based lattice structures with varying aspect ratio in the loading direction, Adv. Sci. Technol. Res. J. 19 (2025) 55–64. https://doi.org/10.12913/22998624/207748.

[7] G. Epasto, D. Rizzo, L. Landolfi, A.L.H.S. Detry, I. Papa, A. Squillace, Design of monomaterial sandwich structures made with foam additive manufacturing, J. Manuf. Process. 121 (2024) 323–332. https://doi.org/10.1016/j.jmapro.2024.05.033.

[8] M. Nofar, Effects of nano-/micro-sized additives and the corresponding induced crystallinity on the extrusion foaming behavior of PLA using supercritical CO2, Mater. Des. 101 (2016) 24–34. https://doi.org/10.1016/j.matdes.2016.03.147.

[9] M. Nofar, A. Tabatabaei, C.B. Park, Effects of nano-/micro-sized additives on the crystallization behaviors of PLA and PLA/CO2 mixtures, Polymer 54 (2013) 2382–2391. https://doi.org/10.1016/j.polymer.2013.02.049.

[10] A.R. Damanpack, A. Sousa, M. Bodaghi, Porous PLAs with controllable density by FDM 3D printing and chemical foaming agent, Micromachines 12 (2021) 866. https://doi.org/10.3390/mi12080866.

[11] N.A.A. Hassan, S. Ahmad, R.S. Chen, F.D. Zailan, D. Shahdan, Effect of processing temperature and foaming agent loading on properties of polylactic acid/kenaf fiber composite foam, Mater. Today Proc. 7 (2019) 601–606. https://doi.org/10.1016/j.matpr.2018.12.0130.1016/j.matpr.2018.12.013.

[12] K.N. Gunasekaran, V. Aravinth, C.B. Muthu Kumaran, K. Madhankumar, S. Pradeep Kumar, Investigation of mechanical properties of PLA printed materials under varying infill density, Mater. Today Proc. 45 (2021) 1849–1856. https://doi.org/10.1016/j.matpr.2020.09.041.